TRENDS IN SCIENCES 2026; 23(10): 13254
https://doi.org/10.48048/tis.2026.13254
RESEARCH ARTICLE

Blue Emissive Carbon Quantum Dots Derived from Green Tea Leaves Cultivated from Gayo High Land for Quantification of Antibiotics

Cut Mutiah[1,*], Abdurrahman[2], Bustami[2], Erlangga Galih Zulva Nugroho[2] and Muhammad Nazar[3]

[1]*Department of Midwifery, Politeknik Kesehatan Aceh, Aceh 23231, Indonesia*
[2]*Department of Nursing, Politeknik Kesehatan Aceh, Aceh 23231, Indonesia*
[3]*Department of Chemistry Education, Universitas Syiah Kuala, Banda Aceh 23111, Indonesia*

([*]Corresponding author's e-mail: cut.mutiah@poltekkesaceh.ac.id)

Received: 3 January 2026, Revised: 5 March 2026, Accepted: 15 March 2026, Published: 20 April 2026

Abstract

Carbon Quantum Dots (CQDs) have emerged as highly attractive nanomaterials in recent decades due to their rapid, cost-effective performance in chemical detection through fluorescence quenching. This study aims to synthesize CQDs from green tea leaves (GTL-CQDs) and utilize them as sensors for antibiotics. The CQDs were synthesized using a hydrothermal method at 180 °C for 4 in an oven, followed by purification, and characterization. The synthesized GTL-CQDs exhibited an average particle size of approximately 10.5 nm. UV-Vis and fluorescence spectroscopy analyses revealed that the CQDs strongly absorb UV light with a maximum absorption peak at 273 nm, and emit visible light in the wavelength range of 350 - 550 nm, with an emission peak centered at 430 nm. The CQDs were employed to test their selectivity toward the detection of various antibiotics, including amoxicillin, cefixime, and ciprofloxacin. The GTL-CQDs were found to be effective in detecting the selected antibiotics but demonstrated greater selectivity toward cefixime with a limit of detection (LOD) of 0.11 $mg \cdot L^{-1}$ or equivalent to 243 nM. Sensing application in real samples (tap water and river water) recoveries 98.90% - 113.35% with RSD $\leq$ 0.19 confirmed the accuracy of cefixime quantification. The developed probe enables reliable, sustainable, and efficient on-site detection of cefixime for environmental monitoring.

Keywords: Carbon Quantum Dots (CQDs), Matcha leaves, Green tea leaves, Antibiotics sensor, Quantification

Introduction

Carbon quantum dots (CQDs) are a class of zero-dimensional carbon materials with diameters typically below 10 nm, which have gained significant popularity over the past few decades due to their fluorescence properties [1]. Generally, CQDs are defined as nanoscale carbon particles exhibiting unique characteristics, including strong fluorescence, high chemical stability, and biocompatibility [2-4]. CQDs were initially discovered as byproducts during the synthesis of other carbon-based nanomaterials [5,6]. Structurally, CQDs comprise an amorphous or semi-crystalline carbon core decorated with oxygen-containing functional groups on their surface, which impart hydrophilicity and specific chemical reactivity.

Among the key features of CQDs, their unique optical properties are considered as the most notable [7]. CQDs exhibit unique and remarkable optical properties that are primarily attributed to their nanoscale dimensions, carbon core structure, and surface functional groups [8]. In terms of absorption, CQDs display strong peaks in the UV to visible light range, arising from electronic transitions such as $\pi \rightarrow \pi^*$ transitions in C=C bonds and $n \rightarrow \pi^*$ transitions in carbonyl groups [9]. Their fluorescence emission is one of their most prominent features, with the emission wavelength being excitation-dependent and exhibiting a significant Stokes shift [10]. This fluorescence originates from several mechanisms, including excitation recombination, surface transitions, and

structural defects. Additionally, the fluorescence color of CQDs can be tuned by altering particle size or by modifying their functional groups; smaller particles tend to emit blue light, whereas larger particles emit green or red light. The high fluorescence stability of CQDs renders them resistant to photobleaching, making them suitable for repeated applications in bioimaging and sensing [11]. CQDs are also environmentally sensitive, with their fluorescence being affected by factors such as pH or specific metal ions, such as Fe^{2+}/Fe^{3+} [12], and Cd^{2+} [13,14], enabling their use as pH sensors or in heavy metal detection. Furthermore, CQDs demonstrate nonlinear optical properties, including 2-photon absorption, which are relevant for laser technologies and high-resolution imaging [15]. The combination of quantum confinement effects, carbon structure, and functional groups provides exceptional versatility for a wide range of scientific and technological applications.

The active functional groups on the surface of CQDs, such as carbonyl (C=O), hydroxyl (−OH), and carboxyl (−COOH), play a critical role in their ability to absorb UV light and emit visible light [16]. These functional groups make CQDs a promising platform for detecting a wide range of chemical substances. They enable specific interactions with target molecules through processes such as metal ion binding, redox reactions, or the formation of chemical complexes [17,18]. For instance, CQD fluorescence can be quenched or enhanced upon interaction with heavy metal ions such as Fe (III), Hg (II), and Pb (II), facilitating rapid and sensitive detection of heavy metals [19-21]. Additionally, CQDs can also detect organic compounds, such as pesticides, pharmaceuticals, or hazardous dyes [22], through changes in their fluorescence properties induced by interactions with these molecules. This capability makes CQDs highly relevant for applications in cosmetics [23], food safety, environmental monitoring, and pharmaceutical analysis, including the detection of trace antibiotic compounds [14,24,25].

The detection of trace amounts of antibiotics is crucial for several interconnected reasons. In the environment, antibiotics from healthcare, agriculture, and aquaculture can enter water bodies and soil, leading to contamination [26]. Even at low concentrations, these residues can disrupt ecosystems, harming aquatic life and beneficial soil microorganisms. Over time, such contamination can result in the accumulation of antibiotics in the food chain, posing risks to both wildlife and human health. Public health is another critical factor [27], trace antibiotic residues in food, water, and the environment can cause adverse health effects, including allergic reactions, organ toxicity, and other long-term complications. Moreover, prolonged exposure to sub-therapeutic antibiotic levels may contribute to antimicrobial resistance (AMR) [28]. This phenomenon, where bacteria evolve to resist antibiotic treatments, is exacerbated by the presence of even minimal antibiotic residues in the environment. AMR represents a significant global health crisis, making common infections harder to treat and increasing the risk of severe outcomes [29].

Regulatory compliance and food safety further underscore the need for detecting trace antibiotics. Governments and international bodies enforce stringent limits on antibiotic residues in food and other consumables to protect consumers and ensure fair trade practices [30]. Accurate monitoring enables producers to meet these regulations and fosters trust in food and water supplies. Overall, efficient detection methods, such as sensors based on CQDs, are crucial tools for protecting ecosystems, safeguarding public health, and mitigating the spread of AMR. In this work, the detection of 3 commonly administered antibiotics, including amoxicillin, cefixime, and ciprofloxacin were conducted using a relatively low-cost UV-Vis spectrophotometer to avoid the higher laboratory costs associated with the use of a fluorescence spectrophotometer.

Materials and methods

Chemicals and green tea leaves sample

Deionized water, ethanol (96%), amoxicillin, cefixime, ciprofloxacin, NaCl, $NaNO_3$, and CH_3COOH were purchased from a local pharmacy of the city of Banda Aceh, Aceh Province, Indonesia. All chemicals unless previously stated were used as received without further purification. The green tea leaves were obtained from Gayo Highland, Central Aceh Regency at the coordinate: 4°34'52.8"N 96°53'10.8"E.

Green tea leaves extraction

Green tea extraction using ethanol via maceration was conducted to isolate bioactive compounds and was

performed according to Ngoc *et al.* [31] with slight modification. Fifty g of dried green tea leaves were accurately weighed and ground into a fine powder using a mortar and pestle. This step aimed to increase the surface area for efficient interaction between the plant material and the solvent. Ethanol (96%) was used to extract both polar and semi-polar compounds from the green tea. The maceration process was performed by immersing the powdered green tea in a 1:10 (w/v) ratio of the ethanol solution in a 500 mL conical flask. The flask was sealed and kept at ambient temperature (25 ± 2 °C) for 48 h to ensure adequate extraction. During this period, the mixture was stirred intermittently every 6 - 8 h to enhance solvent penetration and facilitate the dissolution of phytochemicals. Following the maceration period, the mixture was filtered using filter paper and a funnel to separate the liquid extract from the plant residue. The filtrate was then concentrated using a rotary evaporator at 40 ± 2 °C under reduced pressure, which removed the ethanol and yielded a semi-solid extract rich in bioactive constituents. The final concentrated extract was transferred into an amber glass container and stored at 4 °C to preserve its chemical stability. This extract was prepared for further analysis and synthesis of GTL-CQDs.

Synthesis of GTL-CQDs

GTL-CQDs were prepared by thermal decomposition [32] with minor modifications. To prepare the GTL solution, 20 mL of deionized water was mixed with 1 g of concentrated GTL extract in a hydrothermal autoclave. The solution was heated at a constant temperature of 180 °C for 4 h. The resulting brownish liquid was then allowed to cool naturally to ambient temperature overnight. The products were then centrifuged at 2,000 rpm for 60 min, filtered using filter paper, diluted in deionized water, and the GTL-CQDs were filtered using a 0.22 μm membrane filter to obtain a homogeneous particle size. Further work and analysis were performed using the diluted GTL-CQDs.

Morphology and particle size analysis using HRTEM

The morphology and particle size of the synthesized CQDs were analyzed using high-resolution transmission electron microscopy (HRTEM). To prepare the sample, a dilute aqueous dispersion of CQDs (approximately 0.5 - 1.0 mg/mL) was sonicated for 10 - 15 min to ensure uniform dispersion and minimize aggregation. A small volume of the solution (around 5 μL) was drop-cast onto a 300-mesh copper grid coated with a carbon support film, followed by air drying at room temperature for 12 - 24 h. The dried grid was then inserted into the HRTEM instrument and examined under an accelerating voltage of 200 kV. High-resolution images were captured to observe the particle morphology, distribution, and lattice structures. Particle size measurements were conducted using image analysis software, where diameters of at least 100 individual nanoparticles were measured to determine the average size and distribution. Lattice fringes observed in the HRTEM images were used to estimate the interplanar spacing (d-spacing), providing information on the crystallinity and graphitic nature of the CQDs. This method allowed for a detailed assessment of the nanostructure, confirming the successful synthesis of well-dispersed, nanoscale carbon dots.

Chemical analysis using FTIR

FTIR spectroscopy (Shimadzu IR-Prestige 21) was employed to identify the functional groups present in both the green tea leaf (GTL) extract and the synthesized GTL-CQDs. Prior to analysis, the dried GTL extract and freeze-dried CQDs powder were finely ground and mixed with spectroscopic-grade KBr in an approximate ratio of 1:100 (w/w). The mixtures were then pressed into thin, transparent pellets using a hydraulic press under vacuum. The FTIR spectra were recorded using a Bruker Tensor 27 spectrometer in the range of 4,000 - 400 cm^{-1} with a resolution of 4 cm^{-1}, and each spectrum was averaged over 32 scans to improve signal-to-noise ratio. The spectra of the GTL extract were used to identify the original phytochemical functional groups, such as hydroxyl, carbonyl, and aromatic moieties, while the spectra of GTL-CQDs provided insight into the surface chemistry of the carbon dots, highlighting any chemical modifications or retention of functional groups from the precursor. Comparative analysis of both spectra allowed for the evaluation of chemical transformations occurring during the carbonization and passivation processes, particularly the formation of oxygen- and nitrogen-containing surface functionalities that are critical for the solubility and photoluminescence behavior of the CQDs.

Optical stability of GTL-CQDs

To evaluate the optical stability of the GTL-CQDs, 2 sets of experiments were conducted: pH-dependent stability and photostability under prolonged light exposure. For the pH-dependent analysis, a series of GTL-CQDs aqueous solutions were adjusted to pH values ranging from 2 to 11 using 0.1 M HCl and 0.1 M NaOH. Each solution was allowed to equilibrate for 30 min at room temperature before recording its UV-Vis absorption spectrum using a Shimadzu UV-2,600 spectrophotometer in the wavelength range of 200 - 800 nm. For photostability testing, 2 identical GTL-CQDs solutions (pH = 7) were prepared and placed in quartz cuvettes; one was exposed to continuous UV irradiation at 295 nm using a UV transilluminator (power = 8 W) and the other was exposed to ambient sunlight under clear sky conditions. Both exposures were carried out for a total of 8 hours. At 1-hour intervals, aliquots were withdrawn and their UV-Vis absorbance spectra were recorded immediately without dilution. The stability was evaluated by monitoring changes in absorbance intensity, particularly at the characteristic absorption peak around 270 nm, which is indicative of π–π* transitions in aromatic domains. A minimal change in absorbance over time was taken to indicate high optical stability, while a significant decrease or spectral shift was interpreted as photodegradation or structural transformation of the CQDs under light exposure or extreme pH conditions.

Preparation of antibiotic samples

Each tablet of amoxicillin, cefixime, and ciprofloxacin was dissolved in 100 mL of ethanol to prepare the stock solutions. These stock solutions were subsequently diluted to obtain a concentration of 100 $mg \cdot L^{-1}$ for each antibiotic. Further serial dilutions were carried out to achieve concentrations suitable for sensing experiments. After repeated trials to determine the optimal concentration range for sensor performance using GTL-CQDs, the ideal working concentrations were established as follows: 0.5 - 4 $mg \cdot L^{-1}$ for amoxicillin, 0.15 - 1.2 $mg \cdot L^{-1}$ for cefixime, and 1.5 - 11 $mg \cdot L^{-1}$ for ciprofloxacin.

Antibiotic sensing characteristics of GTL-CQDs

To evaluate the selectivity of the antibiotic sensor, 5 mL of a diluted CQDs solution with an absorbance below 1.0 a.u was prepared. Subsequently, varying concentrations of each antibiotic solution were added to the CQDs solution, and absorbance measurements were performed over the wavelength range of 200 - 800 nm. A gradual decrease in absorbance intensity at 273 nm with increasing antibiotic concentration indicated an interaction and confirmed the sensing capability of the CQDs.

Feasibility test and recovery analysis in real water samples

The feasibility of the proposed CQD-based sensor for antibiotic detection in real samples was evaluated using tap water and spiked environmental water samples. Tap water was collected from the laboratory supply, while environmental water samples (river water) were collected in clean polyethylene bottles from the following coordinate: 5°34'18.8"N 95°21'37.3"E, and filtered through a 0.45 μm membrane filter to remove suspended particulates. All samples were stored at 4 °C and analyzed within 24 h. Prior to analysis, the pH of the samples was adjusted to the optimal sensing pH determined in the selectivity study. Serial concentrations (10 - 50 $mg \cdot L^{-1}$) of cefixime were spiked into the water samples within the linear detection range of the CQD sensor. Unspiked samples were analyzed in parallel as blank controls to assess matrix interference.

For spectrometric measurements, an aliquot of CQD solution was mixed with the spiked or unspiked water sample in a ratio of 1:1 and incubated for an optimized interaction time at ambient temperature. The UV Vis spectra were recorded under 273 nm, and the absorbance intensity change (ΔA or A/A_0) was used to quantify the antibiotic concentration based on the calibration curve obtained in deionized water. The recovery percentage was calculated using the Eq. (1).

$$Recovery\ (\%) = \frac{(C_{spiked} - C_{unspiked})}{C_{added}} \times 100 \quad (1)$$

All measurements were performed in triplicate, and the results were reported as mean recovery ± standard deviation (SD).

Results and discussion

The CQDs were successfully synthesized from green tea leaves through a simple and environmentally friendly hydrothermal method. The obtained CQDs were subsequently characterized using various techniques to determine their morphological and optical properties. HRTEM analysis revealed a uniform particle size distribution at the nanometer-scale with nearly spherical shapes. The UV-Vis spectrum exhibited a characteristic absorption band in the ultraviolet region, indicative of π-π* transitions of aromatic C=C bonds, while fluorescence (FL) spectroscopy demonstrated strong and stable emission in the visible range, confirming the potential of these CQDs for applications in various fields.

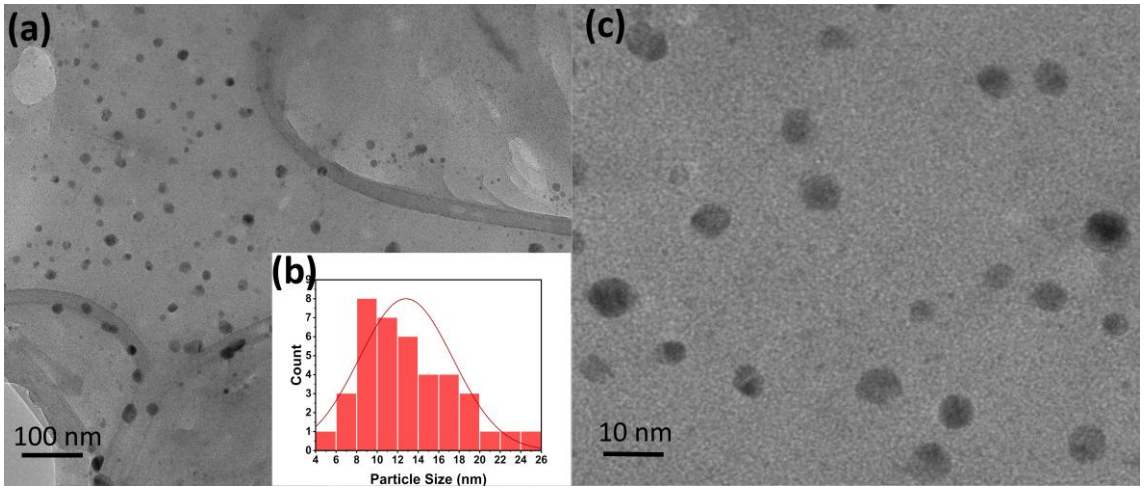

Figure 1 TEM images of GTL-CQDs with different magnifications (a) 10,000× (c) 50,000× and (b) the inset of particle size distribution.

Figure 1 presents a HR-TEM image of GTL-CQDs at different magnifications. The micrograph reveals a substantial number of discrete, quasi-spherical nanoparticles, uniformly dispersed across the supporting carbon grid. The particles exhibit strong contrast against the background, indicating well-defined, dense carbonaceous structures with high electron density. This morphology is characteristic of CQDs and supports the successful formation of carbon-based nanostructures. The scale bar of 100 nm suggests that the individual particles are within the nanometer range, primarily between 5 and 20 nm in diameter. Furthermore, the images suggest minimal visible agglomeration, which implies good dispersibility and colloidal stability traits commonly attributed to the surface functional groups introduced during green synthesis using phytochemicals such as polyphenols, catechins, and flavonoids from green tea leaves [33]. These bioactive molecules can act as both carbon sources and natural passivating agents, contributing to the uniformity and stability of the CQDs [34].

Figure 1(b) illustrates the particle size distribution histogram, obtained by measuring the diameters of a statistically significant number of individual CQDs from the TEM image. The data show a Gaussian-like distribution with a peak (mode) centered around 8 - 10 nm, which represents the most frequently occurring size class. The particle sizes range broadly from approximately 4 to 21 nm, indicating a relatively narrow but not monodisperse size distribution. The slight asymmetry in the distribution tail suggests the presence of a small number of larger particles, which is common in biomaterial-derived nanostructures due to the inherent variability in natural precursors [35]. Importantly, the use of green tea as a precursor introduces eco-friendly, low-cost, and non-toxic advantages, aligning with the principles of green chemistry [36-38]. The abundant phytochemicals present in green tea likely play multiple roles in the synthesis process: Acting as reducing agents, carbon donors, and surface passivators [39,40]. This integrated role not only simplifies the synthetic route - requiring fewer external reagents or stabilizers - but also

contributes to the observed monodispersity and colloidal stability of the resulting CQDs.

Furthermore, the average particle size below 10 nm (**Figure 1(b)**) is particularly advantageous for several applications. In bioimaging and biosensing, smaller CQDs typically exhibit stronger fluorescence, higher surface-to-volume ratios, and better tissue permeability [41-43]. In addition, the presence of surface functional groups originating from green tea (e.g., hydroxyl, carboxyl, or amine groups) enhances the solubility in aqueous media and provides accessible sites for chemical functionalization, enabling their use in targeted drug delivery [17,44], metal ion sensing, or environmental pollutant detection [45,46].

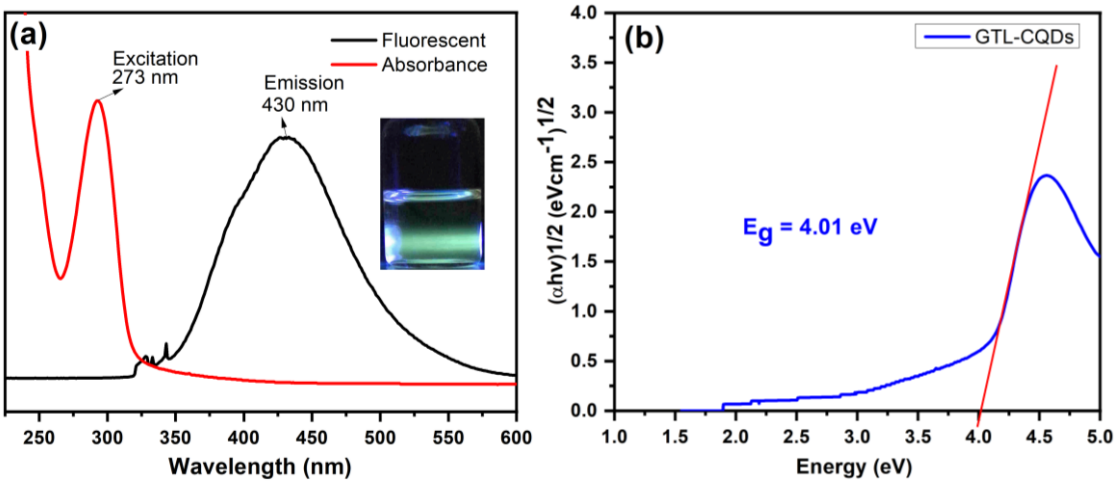

Figure 2 (a) Absorbance and fluorescent intensity of GTL-CQDs (the inset image of GTL-CQDs observed under UV light at 365 nm), (b) indirect energy band gap of the GTL-CQDs estimated using Tauc plot.

The optical properties of GTL-CQDs were analyzed using a UV-Vis spectrophotometer where the absorbance was measured over the wavelength range of 200 to 600 nm, and a fluorescence spectrophotometer at different excitation wavelengths from 250 to 400 nm with 10 nm increments. CQDs typically exhibit excellent UV absorbance within the range of 200 - 300 nm, attributed to chromophores with double bonds, such as C=C and C=O [47,48]. The GTL-CQDs synthesized in this study showed a maximum absorption peak at a wavelength of 273 nm and an emission peak at 430 nm, as indicated by the UV-Vis spectrum and the fluorescence spectrum presented in **Figure 2(a)**. The optical characterization of GTL-CQDs revealed their strong UV absorption and blue fluorescence emission, characteristic features of CQDs. These properties stem from their inherent carbon-based structure and surface functional groups, which enable electronic transitions and efficient fluorescence [18,49]. The UV absorption at 273 nm and the fluorescence emission at 430 nm observed in GTL-CQDs are direct consequences of their quantum-confined energy band gap of 4.01 eV, as depicted in **Figure 2(b)**. Because GTL-CQDs are nanoscale, their electrons and holes occupy discrete energy levels rather than continuous bands. The gap between the valence and conduction levels corresponds to the energy of UV light around 273 nm, which they effectively absorb through $\pi \rightarrow \pi^*$ and $n \rightarrow \pi^*$ transitions involving C=C and C=O chromophores [1,50]. When these excited electrons relax back to lower energy states, they emit blue light as depicted in the inset photo of **Figure 2(a)**.

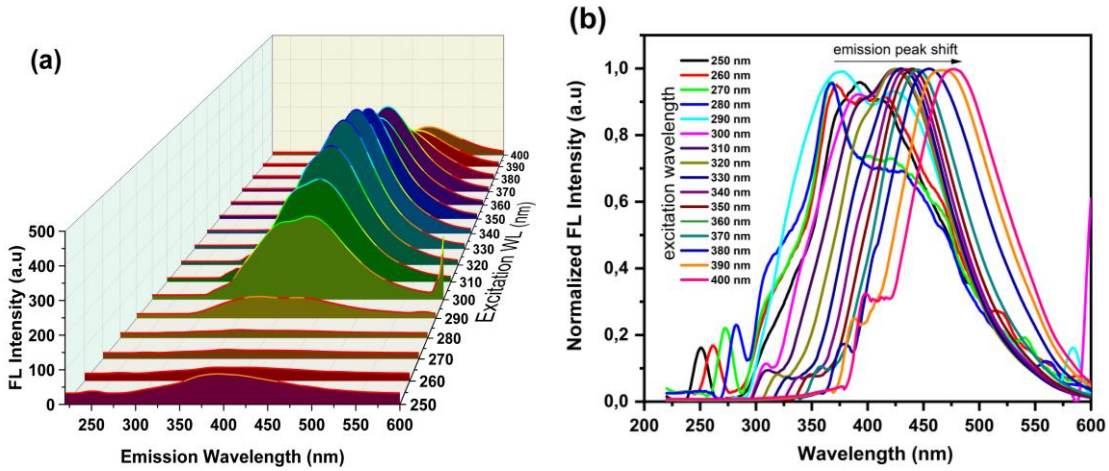

Figure 3 (a) excitation-dependent FL spectra of GTL-CQDs, and (b) normalized FL intensity confirming the emission peak shift due to varied excitation wavelength.

The fluorescence analysis of GTL-CQDs with excitation wavelengths ranging from 250 to 400 nm reveals excitation-dependent fluorescence, with a maximum emission at an excitation wavelength of 330 nm (**Figure 3(a)**). The variation in the excitation wavelength also causes the emission peak to shift to longer wavelengths as the excitation wavelength increases (**Figure 3(b)**). This common phenomenon of CQDs arises from several factors, including the distribution of particle sizes, surface states, structural defects, and the efficiency of energy transfer [51,52]. Smaller particles with larger band gaps emit light at shorter wavelengths, while larger particles emit at longer wavelengths [53]. Surface functional groups such as C=O, −OH, and −COOH introduce localized electronic states that interact differently depending on the excitation energy, resulting in varied emission intensities and wavelengths [54,55]. Structural defects, such as irregularities in the carbon lattice or the incorporation of heteroatoms, create additional energy levels that contribute to wavelength-specific emissions [56]. Furthermore, lower-energy excitations may only activate specific transitions, leading to distinct fluorescence outputs compared to higher-energy excitations. These excitation-dependent properties highlight the complexity of the electronic structure of GTL-CQDs and expand their potential for applications in multicolor fluorescence detection, bioimaging, and optical technologies, where tunable light emission is crucial [57].

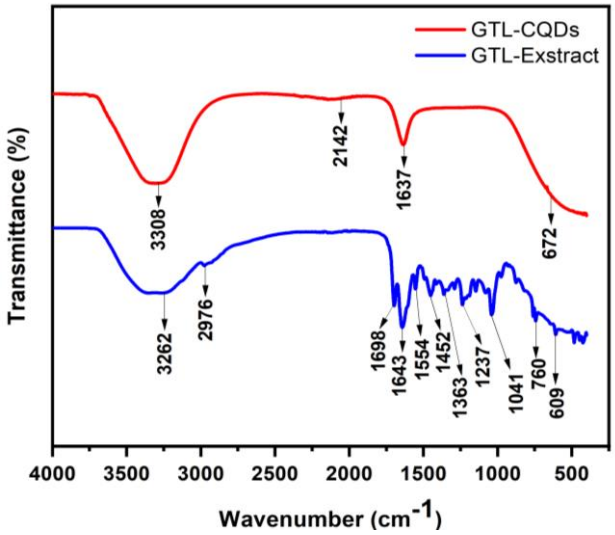

Figure 4 FTIR spectra of GT-Extract and the GTL-CQDs.

The FTIR spectra of the GTL extract and GTL-CQDs in **Figure 4** reveal significant insights into the chemical transformations that occur during the carbonization process and the functional groups retained on the CQD surface. A broad and intense absorption band observed around 3,200 - 3,500 cm^{-1} in both spectra corresponds to the O–H stretching vibrations of hydroxyl groups and possible N–H stretching from amine-containing compounds [58]. This peak remains broad and pronounced in the CQD spectrum, indicating the retention of polar functional groups such as hydroxyls and amines, which contribute to the hydrophilicity and dispersibility of the carbon dots in aqueous media [59]. In the region of 2,800 - 3,000 cm^{-1}, both spectra exhibit weak bands associated with aliphatic C–H stretching vibrations from $–CH_2$ and $–CH_3$ groups. However, these bands are slightly reduced in intensity in the CQDs spectrum, suggesting partial degradation of long-chain aliphatic structures during the synthesis [60]. A notable peak near 1,700 cm^{-1} is evident in both spectra, assigned to the C=O stretching vibrations of carbonyl or carboxyl groups. In the CQDs, this peak becomes more defined and slightly shifted, indicating the formation or enrichment of carboxylic acid functionalities, likely as a result of oxidative cleavage of polyphenols and other oxygenated compounds in the GTL extract.

The region from 1,500 to 1,650 cm^{-1} in the GTL extract shows multiple absorptions attributed to aromatic C=C stretching vibrations and amide bonds, possibly arising from polyphenolic structures and protein residues. In the CQDs, the peaks in this region are attenuated or altered, which is consistent with the partial breakdown and restructuring of aromatic rings and nitrogen-containing compounds during hydrothermal treatment [61,62]. Meanwhile, the presence of peaks in the range of 1,000 - 1,300 cm^{-1} in both samples corresponds to C–O and C–N stretching vibrations, reflecting the presence of alcohols, ethers, and amines. These functional groups persist in the CQDs, supporting the incorporation of oxygen- and nitrogen-containing moieties on the particle surface [63]. In the fingerprint region below 1,000 cm^{-1}, the GTL extract displays a series of complex, sharp peaks typical of various phytochemical skeletons, including flavonoids and alkaloids. In contrast, the CQDs spectrum is smoother and less complex in this region, which may be attributed to the decomposition of complex biomolecules and the formation of more uniform carbonaceous frameworks during carbon dot synthesis [64]. Overall, the FTIR analysis confirms that while the GTL-CQDs retain several surface functionalities inherited from the precursor, including hydroxyl, carbonyl, and amine groups, the carbonization process also introduces structural simplification and new functional groups essential for the optical and chemical properties of the CQDs.

Optical stability of GTL-CQDs

The optical stability of GTL-CQDs was evaluated under varying pH conditions and exposure to UV light and sunlight over an extended period. In solutions with different pH values, the GTL-CQDs exhibited notable changes in their UV-Vis absorption spectra as the pH increased, while maintaining excellent stability under acidic conditions. On the other hand, when subjected to UV light at 295 nm for 8 h, the absorbance intensity in the UV region (250 - 300 nm) remained relatively unchanged, showcasing their photostability. Furthermore, exposure to direct sunlight for 8 h did not result in a significant reduction in absorbance intensity, reflecting their excellent resistance to photodegradation. These findings highlight the robust structural and chemical properties of GTL-CQDs, making them suitable for applications requiring high optical stability under diverse environmental conditions.

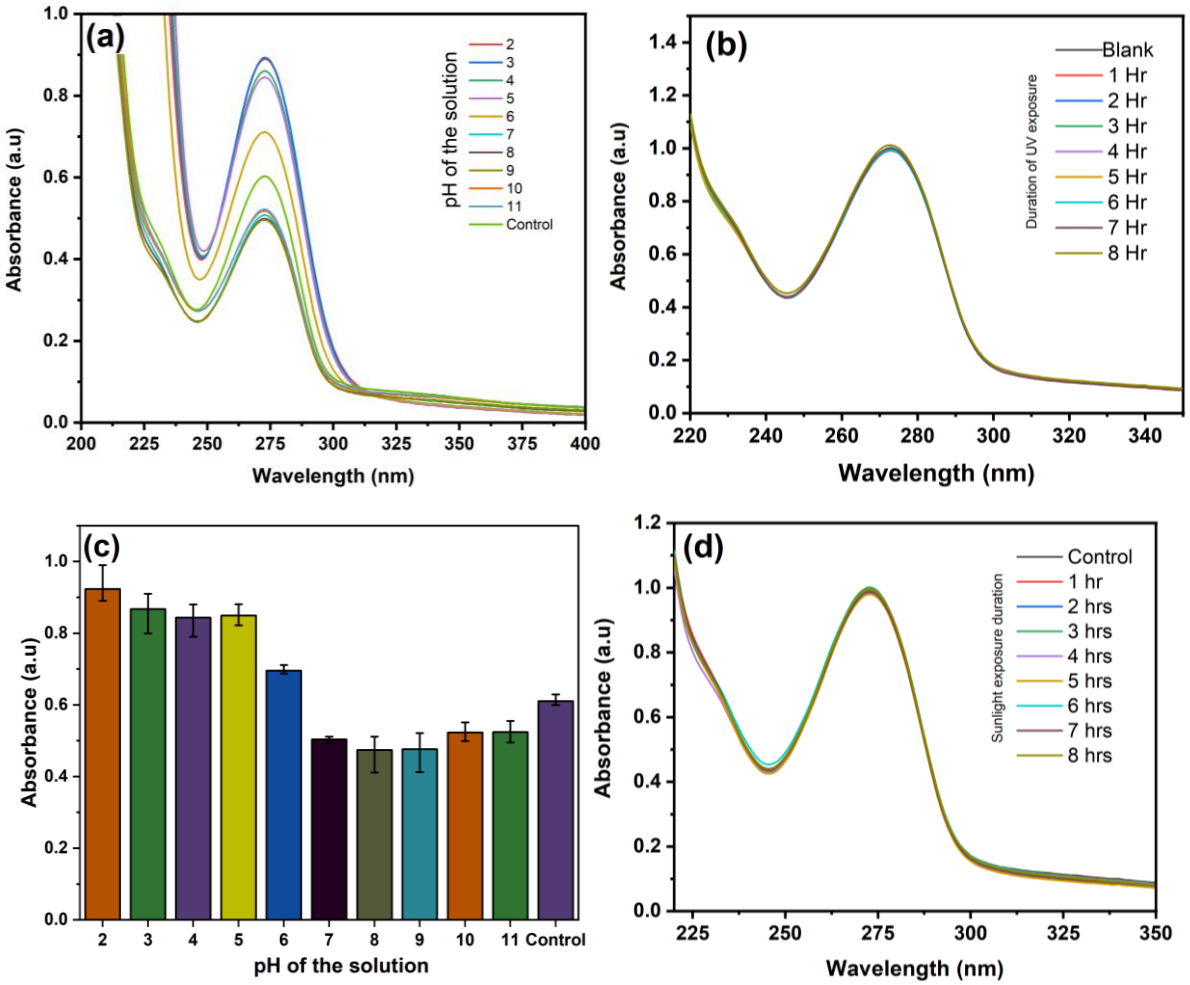

Figure 5 (a) pH-dependent UV-Vis spectra of GTL-CQDs, (b) absorbance of GTL-CQDs after being exposed to UV (365 nm) at different durations, (c) pH-dependent absorbance of GTL-CQDs at the maximum peak (273 nm), and (d) the UV-Vis spectra of GTL-CQDs after sunlight exposure.

Figure 5 illustrates the results of the stability test of CQDs against changes in the environmental pH of the solution, as well as the optical stability of GTL-CQDs under UV light and sunlight exposure for 0 - 8 h. The UV-Vis spectra in Figure 5a show that the solvent's pH affects the UV absorption by GTL-CQDs, with relatively higher UV absorption observed at low pH levels (2 - 6) as illustrated in Figure 5c. The UV absorption decreases as the pH of the solution increases. CQDs often exhibit stronger UV absorption at lower pH levels primarily due to changes in their surface chemistry and electronic structure [65]. At low pH, acidic conditions lead to the protonation of surface functional groups such as carboxyl (−COOH), hydroxyl (−OH), and amino ($-NH_2$). This protonation alters the electronic environment of the CQDs, enhancing their ability to absorb UV light [66]. The protonated groups create new pathways for electronic transitions, including $\pi \rightarrow \pi^*$ and $n \rightarrow \pi^*$ transitions, thereby increasing the efficiency of UV absorption. Additionally, protonation can reduce the bandgap of CQDs, modifying their energy levels to favor stronger absorption in the UV region. Furthermore, lower pH can influence the aggregation behavior of CQDs [67]. Acidic conditions reduce the electrostatic repulsion between particles, enabling them to approach one another and form aggregates. This aggregation can intensify UV absorption due to the increased interaction of light with closely packed particles. Simultaneously, the stabilization of surface defects or functional groups under acidic conditions can quench non-radiative recombination pathways, leading to more effective absorption in the UV spectrum [68].

The GTL-CQDs were found to be optically stable when exposed to UV light and natural sunlight up to 8 h during daylight. The UV-Vis measurements revealed negligible changes in the UV absorption capability of the CQDs after exposure to UV light at a wavelength of 295 nm for 8 h. The absorbance intensity in the UV region, specifically in the wavelength range of 250 - 300 nm, remained relatively stable without any notable decrease, as shown in **Figure 5(b)**. Similarly, the durability of the GTL-CQDs under sunlight exposure demonstrated excellent stability, with no significant reduction in absorbance intensity observed after continuous exposure to sunlight for 8 h, as shown in **Figure 5(d)**. The stability of GTL-CQDs, under prolonged UV and sunlight exposure, is primarily due to their robust carbon core structure, which resists photodegradation [69]. Functional groups such as hydroxyl (−OH) and carboxyl (−COOH) on the CQD surface act as a passivating layer, shielding the material from oxidative and photochemical damage [60]. Additionally, CQDs efficiently dissipate absorbed UV energy through fluorescence emission or non-radiative processes, preventing energy buildup that could lead to structural damage [70]. Their nanoscale size and quantum confinement effects further enhance optical stability, while their high thermal and chemical resilience ensures consistent performance under varying environmental conditions [71-73].

Antibiotic-sensing properties of GTL-CQDs

In recent years, CQDs have attracted considerable interest as versatile nanomaterials for chemical sensing, particularly due to their ease of synthesis, biocompatibility, surface tunability, and strong optical responses [74,75]. Their application in antibiotic detection has become increasingly important given the widespread occurrence of pharmaceutical residues in environmental and clinical settings. In this study, GTL-CQDs were utilized in sensing selected antibiotics. Unlike many previous studies that rely on expensive fluorescence spectroscopy, this research employed a low-cost UV-Vis spectroscopy to monitor the interactions between CQDs and selected antibiotics - amoxicillin, cefixime, and ciprofloxacin. The sensing mechanism was based on a measurable decrease in the UV-Vis absorption peak of the CQDs at 273 nm, which diminished progressively with increasing concentrations of the antibiotics. This spectral change provides a straightforward and sensitive approach for quantifying these pharmaceutical compounds. This subsection presents the detailed data and analytical evaluation of the green tea leaf-derived CQDs in detecting each antibiotic.

The absorbance reduction measurements of the CQDs following the addition of antibiotics at varying concentrations revealed a consistent decreasing trend, as illustrated in **Figures 6(a) - 6(c)**. Several rounds of trial and error were conducted to determine the ideal absorbance condition of the CQDs for evaluating their interactions with each antibiotic. As a result, the antibiotic concentrations used in this study differ from one another to ensure the accuracy of the measurements. The concentration ranges employed were 0.5 - 4 $mg \cdot L^{-1}$ for amoxicillin, 0.15 - 1.2 $mg \cdot L^{-1}$ for cefixime, and 1.5 - 11 $mg \cdot L^{-1}$ for ciprofloxacin. These ranges were established after repeated experiments showed that the amount of antibiotic added influenced the absorbance of CQDs to different extents, depending on the specific antibiotic used. **Figure 6(d)** compares the normalized absorbance response of the sensing system toward target antibiotics in the presence of common ionic interferences (NaCl, $NaNO_3$, and CH_3COONa). Overall, the results clearly demonstrate that simple inorganic salts exert negligible influence on the absorbance signal, whereas antibiotics induce a pronounced and distinguishable response. The 3 ionic species show normalized absorbance values close to unity, with NaCl even slightly exceeding the blank. This behavior indicates that monovalent ions (Na^+, Cl^-, NO_3^- and CH_3COO^-) do not significantly interact with the active sites of the sensing material or perturb its electronic structure [76]. Their weak electrostatic interactions and lack of specific coordination capability prevent them from inducing notable changes in absorbance, confirming strong resistance of the system to ionic strength variations commonly encountered in real water matrices [77].

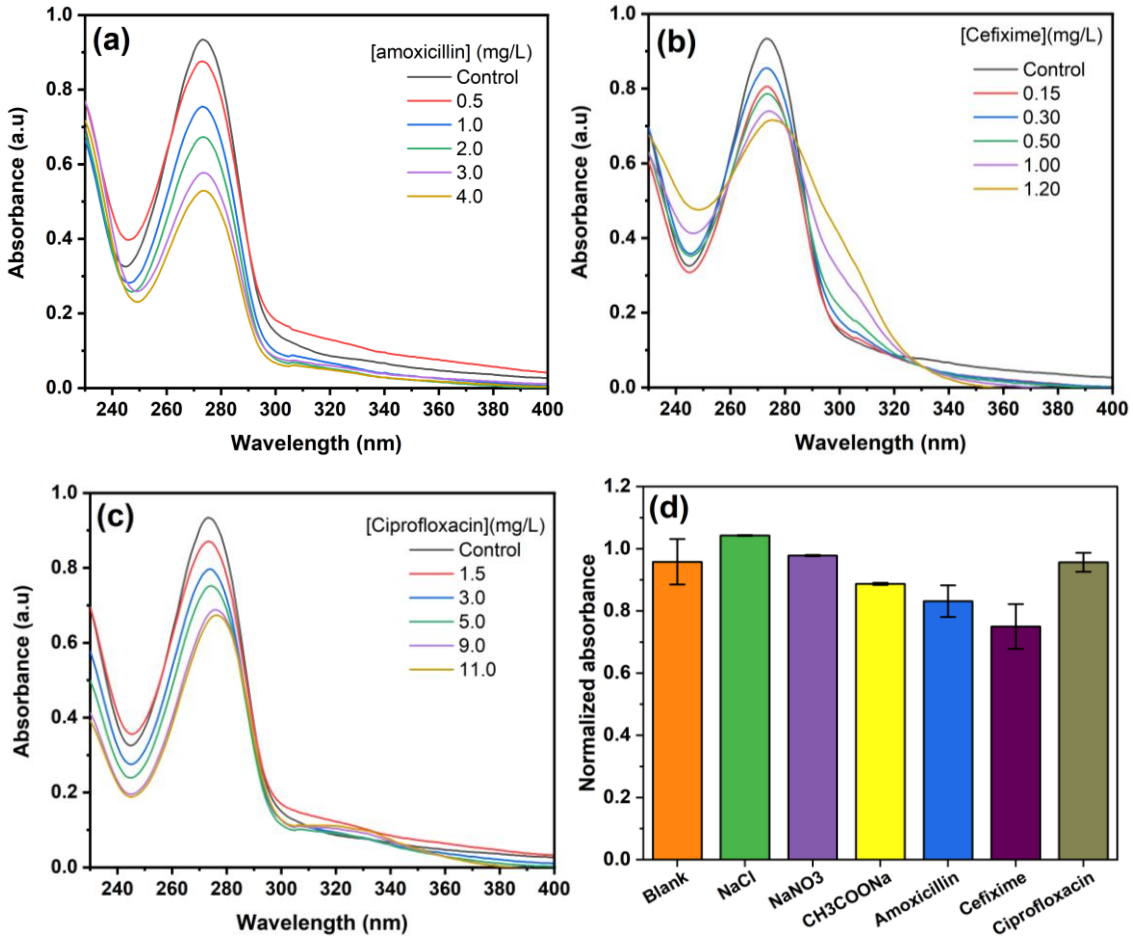

Figure 6 (a) The UV-Vis spectra of GTL-CQDs with the addition of amoxicillin at different concentration, (b) The UV-Vis spectra of GTL-CQDs with the addition of cefixime at different concentration, (c) The UV-Vis spectra of GTL-CQDs with the addition of ciprofloxacin at different concentration, and (d) the normalized absorbance of each antibiotic and interference substances at similar concentrations.

In contrast, the presence of antibiotics leads to a clear decrease in normalized absorbance, with cefixime showing the most pronounced effect, followed by amoxicillin, while ciprofloxacin exhibits a moderate but still significant response. This trend suggests selective interactions between the antibiotics and the sensing material, likely arising from a combination of hydrogen bonding, π–π stacking, and possible charge-transfer interactions involving functional groups such as –NH, –OH, and aromatic rings present in the antibiotic molecules. The stronger response observed for cefixime can be attributed to its more complex molecular structure and higher affinity toward surface functional groups, resulting in enhanced absorbance modulation [78].

After testing various concentration ranges, optimal conditions were achieved as presented in **Figures 7(a) - 7(c)**. The calculated LOD for amoxicillin, cefixime, and ciprofloxacin were found to be 0.45, 0.11, and 0.32 mgL^{-1}, respectively. These values were corroborated by the calibration plots in **Figure 7**, which display a linear regression between absorbance and antibiotic concentration. Notably, the regression plot for cefixime (**Figure 7(b)**) demonstrated the highest degree of linearity with an R^2 value of 0.9952, surpassing those of amoxicillin (R^2 = 0.94537, **Figure 7(a)**) and ciprofloxacin (R^2 = 0.9712, **Figure 7(c)**).

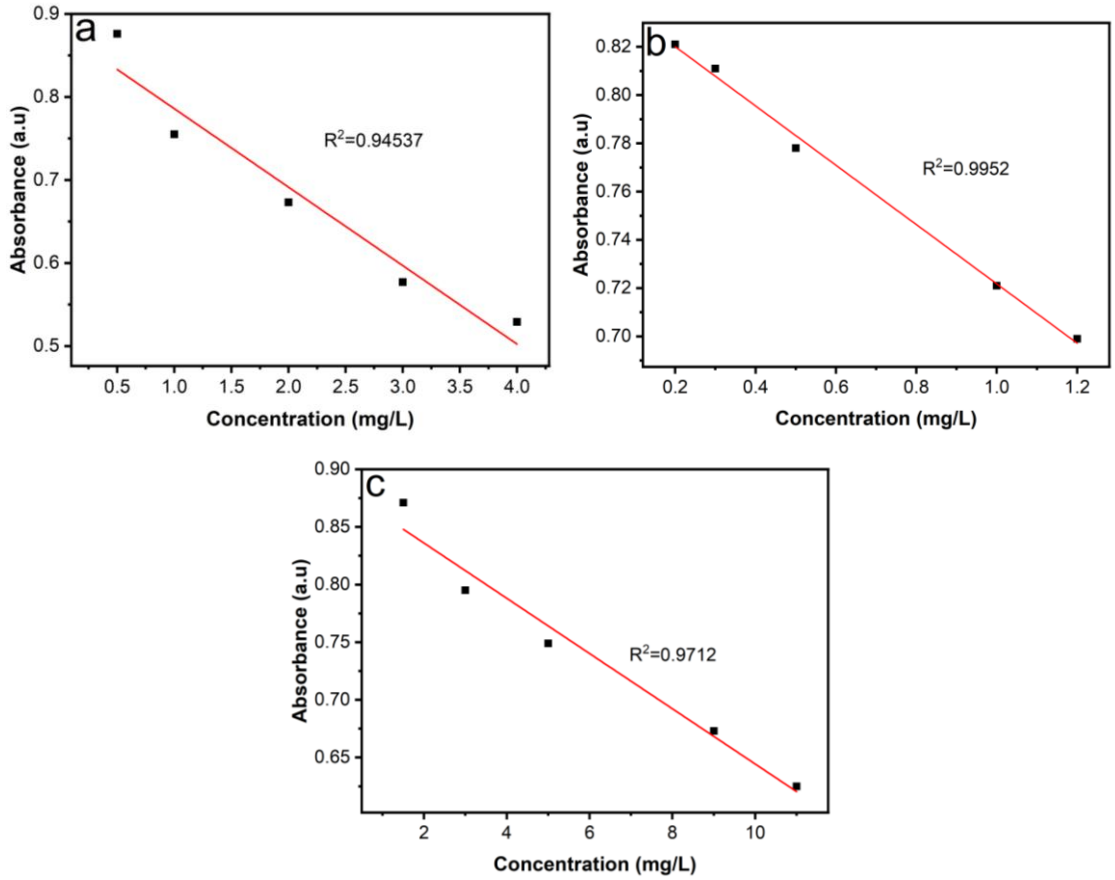

Figure 7 The linear plot of absorbance of CQDs against the antibiotics at increasing concentrations (a) amoxicillin, (b) cefixime, and (c) ciprofloxacin.

Recent studies have revealed that CQDs can be utilized in antibiotic sensing at very low concentrations [32]. This promising application stems from the unique photoluminescent properties of carbon quantum dots (CQDs), which can undergo significant fluorescence changes—either enhancement or quenching - upon interaction with specific antibiotic molecules [79]. These interactions are typically driven by mechanisms such as the inner filter effect (IFE), Förster resonance energy transfer (FRET), and static or dynamic quenching, allowing for precise detection of various antibiotic classes including tetracyclines, fluoroquinolones, and aminoglycosides [80,81].

Notably, the sensitivity of CQD-based sensors is remarkably high. For instance, a recent study demonstrated that nitrogen-doped CQDs could detect tetracycline antibiotics like tetracycline, oxytetracycline, and chlorotetracycline with detection limits as low as 5.18, 6.06 and 14 nM, respectively in complex matrices such as milk and tobacco [82]. In another example, a dual-mode sensor based on Au-CQD nanocomposites achieved detection of gentamicin and kanamycin at approximately 120 - 195 nM, integrating both fluorescence and colorimetric responses for enhanced reliability [83]. These findings not only demonstrate the ultra-sensitive capabilities of CQDs but also their selectivity, which is often enhanced through doping (e.g., with nitrogen, sulfur, or phosphorus) or surface functionalization using polymers or peptides. The full comparison of various antibiotics detections and the precursors used in tabulated in **Table 1**.

Table 1 Comparison of CQDs prepared from different precursors for antibiotic detection.

No	Precursor	Detection method	Target antibiotics	LOD (nM)	Reference
1	Brown granulated sugar and tree leaves	Ratiometric fluorescent	Amoxicillin	2.39	[84]
2	Citric acid and polyethyleneimine	Lateral flow assay	aflatoxin M1	0.21	[85]
3	Citric acid, zirconium chloride, and ethylenediamine	Fluorescence quenching	tetracycline and oxytetracycline	29 and 16	[86]
4	PEI and L-Cys	Ratiometric fluorescence	tetracycline hydrochloride	5.92	[87]
5	Diphenylamine, Eu^{3+}, and 1,2,4,5-benzenetetracarboxylic acid (h4btec)	Ratiometric fluorescence	Tetracycline, oxytetracycline, and doxycycline hydrochloride	73.0, 51.7 and 54.9	[88]
6	Onion and urea	fluorescence, spectrophotometric, smartphone, and test strip	Cefixime	5.16, 138.08, 560 and 650	[89]
7	Ascorbic acid, uric acid, and glucose	Absorbance and fluorescence	Cefadroxil	20 and 4.0	[90]
8	Graphene oxide and gold nanowires	Electro-polymerization	Cefixime	7.1	[78]
9	Green tea leaves	Spectrophotometric	Cefixime	243	This work

Moreover, researchers have embraced green chemistry approaches in synthesizing CQDs, using biomass waste or simple precursors like citric acid and urea through hydrothermal methods [91]. This low-cost, eco-friendly synthesis is not only scalable but also enhances quantum yield and surface reactivity. CQDs integrated with other nanostructures including metal-organic frameworks (MOFs)—have also shown dual-emission or ratiometric properties, allowing visual or wavelength-based discrimination between antibiotics. In practical applications, these CQDs have performed well in detecting antibiotics in real-world samples like honey, chicken feed, tap water, and milk, with high recovery rates (typically 91% - 110%) and excellent accuracy [92,93].

Despite these advances, the transition of CQD-based sensors from laboratory settings to real-time, field-deployable platforms remains a challenge. Issues such as potential interference from sample matrices, variability in synthesis, and long-term photostability need to be addressed. Nonetheless, the future is bright for CQDs as next-generation sensors in food safety, environmental monitoring, and clinical diagnostics, where detecting antibiotics at nanomolar levels is crucial for managing contamination and antibiotic resistance.

Analysis of Cefixime in real water samples

To verify the practical feasibility of the proposed GTL-CQDs fluorescent sensing platform beyond controlled laboratory conditions, its analytical performance was further evaluated using real water samples. Environmental water matrices typically contain diverse dissolved salts, residual disinfectants, and natural organic matter that can potentially interfere with fluorescence-based detection through competitive interactions or signal modulation. Therefore, recovery studies using spiked tap water and river water samples were conducted to systematically assess the accuracy, precision, and matrix tolerance of the GTL-CQDs probe for cefixime quantification.

Table 2 Detecting results of cefixime in real water samples using GTL-CQDs (n = 3).

Water Sample	Spiked con. ($mg \cdot L^{-1}$)	Measured Con. ($mg \cdot L^{-1}$)	Recovery (%)	RSD (%)
Tap water	10	9.89	98.90	0.14
	20	20.91	104.55	0.13
	30	33.21	110.70	0.22
	40	45.34	113.35	0.12
	50	52.76	105.52	0.17
River water	10	10.12	101.20	0.09
	20	20.01	100.05	0.19
	30	31.72	105.73	0.07
	40	42.53	106.33	0.09
	50	49.45	98.90	0.11

The practical applicability of the GTL-CQDs probe for antibiotics was critically assessed through recovery studies in spiked tap water and river water samples (**Table 2**), which represent matrices of increasing chemical complexity. Over the examined concentration range of 10 - 50 $mg \cdot L^{-1}$, the method demonstrated reliable quantitative performance in both matrices, indicating that the fluorescence response of GTL-CQDs toward cefixime is sufficiently robust for real-world aqueous environments. For tap water samples, the close correspondence between measured and spiked concentrations resulted in recoveries ranging from 98.90% to 113.35%, confirming acceptable analytical accuracy. The gradual increase in recovery at higher cefixime levels ($\geq$ 30 $mg \cdot L^{-1}$) suggests a minor positive deviation, which may be attributed to enhanced probe-analyte interactions or cumulative absorbance amplification at elevated analyte concentrations rather than significant matrix-induced interference. Importantly, the remarkably low RSD values ($\leq$ 0.22%, n = 3) indicate excellent repeatability and high signal stability of the GTL-CQDs system, confirming its suitability for routine quantitative analysis [94].

In river water samples, which contain a more complex mixture of dissolved ions and natural organic matter, recoveries remained tightly distributed between 98.90% and 106.33%, with RSD values consistently below 0.19%. This level of accuracy and precision demonstrates the strong matrix tolerance of the sensing platform. The absence of pronounced signal destruction or enhancement effects suggests that common interferents present in natural waters do not competitively interact with the GTL-CQDs surface or perturb the cefixime-induced absorbance response. Consequently, these results highlight the inherent selectivity of GTL-CQDs toward cefixime as a result of specific surface functional group interactions and effective electronic coupling between the antibiotic and the CQD surface functional groups.

Conclusions

The current work has successfully synthesized the monodisperse CQDs from green tea leaves cultivated in the Gayo highlands, Province of Aceh, Indonesia. The GTL-CQDs with an average particle size of 10 ± 0.11 nm exhibit notable optical stability when exposed to UV light up to 8 h and demonstrated excellent stability in acidic solutions. The evaluation of the sensing properties against various antibiotics revealed that GTL-CQDs exhibited selective recognition toward amoxicillin and cefixime, with notably higher sensitivity observed for cefixime with LOD of 0.11 mgL^{-1}. Recovery studies in tap and river water confirm that the GTL-CQDs probe enables accurate, precise, and matrix-tolerant quantification of cefixime, with recoveries close to 100% and very low RSDs, demonstrating its robustness, selectivity, and suitability for reliable antibiotic detection in real aqueous environments.

Acknowledgements

The authors would like to express gratitude to the head of Chemistry Laboratory, Department of Chemistry Education, Universitas Syiah Kuala, Indonesia for spectrometric analysis.

Declaration of Generative AI in Scientific Writing

AI-assisted technologies, including ChatGPT and Grammarly, were utilized during manuscript preparation to enhance readability and language quality.

CRediT author statement

Cut Mutiah: Conceptualization; Methodology; Resources; Writing-Review & Editing. **Abdurrahman**: Data curation; preparation; supervision. **Bustami**: Formal Analysis; Visualization; Investigation. **Erlangga Galih Zulva Nugroho**: Supervision; Validation; Formal Analysis. **Muhammad Nazar**: Software; Methodology; Visualization; Writing - Original draft.

References

[1] SY Lim, W Shen and Z Gao. Carbon quantum dots and their applications. *Chemical Society Reviews* 2015; **44(1)**, 362-381.

[2] L Liu, Z Mi, Q Hu, C Li, X Li and F Feng. Green synthesis of fluorescent carbon dots as an effective fluorescence probe for morin detection. *Analytical Methods* 2019; **11(3)**, 353-358.

[3] R Atchudan, TNJI Edison, KR Aseer, S Perumal and YR Lee. Hydrothermal conversion of *Magnolia liliiflora* into nitrogen-doped carbon dots as an effective turn-off fluorescence sensing, multi-colour cell imaging and fluorescent ink. *Colloids and Surfaces B: Biointerfaces* 2018; **169**, 321-328.

[4] H Lin, J Huang and L Ding. Preparation of Carbon Dots with high-fluorescence quantum yield and their application in dopamine fluorescence probe and Cellular Imaging. *Journal of Nanomaterials* 2019; **2019(1)**, 5037243.

[5] H Liu, Z Li, Y Sun, X Geng, Y Hu, H Meng, J Ge and L Qu. Synthesis of luminescent carbon dots with ultrahigh quantum yield and inherent folate receptor-positive cancer cell targetability. *Scientific Reports* 2018; **8(1)**, 1086.

[6] C Yu, T Xuan, Y Chen, Z Zhao, X Liu, G Lian and H Li. Gadolinium-doped carbon dots with high quantum yield as an effective fluorescence and magnetic resonance bimodal imaging probe. *Journal of Alloys and Compounds* 2016; **688**, 611-619.

[7] Z Zhu, H Niu, R Li, Z Yang, J Wang, X Li, P Pan, J Liu and B Zhou. One-pot hydrothermal synthesis of fluorescent carbon quantum dots with tunable emission color for application in electroluminescence detection of dopamine. *Biosensors and Bioelectronics: X* 2022; **10**, 100141.

[8] SA Al-Ghamdi, AAA Darwish, TA Hamdalla, A Pasha, ME Elnair, A Al-Atawi and S Khasim. Biological synthesis of novel carbon quantum dots using *Halimeda opuntia* green algae with improved optical properties and electrochemical performance for possible energy storage applications. *International Journal of Electrochemical Science* 2023; **18(5)**, 100102.

[9] T Yuan, T Meng, P He, YX Shi, Y Li, X Li, L Fan and S Yang. Carbon quantum dots: An emerging material for optoelectronic applications. *Journal of Materials Chemistry C* 2019; **7(23)**, 6820-6835.

[10] A Vibhute, T Patil, R Gambhir and AP Tiwari. Fluorescent carbon quantum dots: Synthesis methods, functionalization and biomedical applications. *Applied Surface Science Advances* 2022; **11**, 100311.

[11] J Shen, S Shang, X Chen, D Wang and Y Cai. Facile synthesis of fluorescence carbon dots from sweet potato for Fe^{3+} sensing and cell imaging. *Materials Science and Engineering: C* 2017; **76**, 856-864.

[12] J Janshongsawang, N Pimsin, D Nugroho, P Nuengmatcha, P Porrawatkul and S Chanthai. Selective fluorescence quenching sensor for trace determination of iron (Fe^{2+}/Fe^{3+}) in water sample using natural Carbon Dots (CDs) synthesized by microorganisms from leech lime (*Citrus hystrix* DC.) fermentation extract. *Trends in Sciences* 2025; **22(12)**, 10639.

[13] M Nazar, M Hasan, B Wirjosentono, BA Gani and CE Nada. Microwave synthesis of carbon quantum dots from arabica coffee ground for fluorescence detection of Fe^{3+}, Pb^{2+}, and Cr^{3+}. *ACS Omega* 2024; **9(18)**, 20571-20581.

[14] SA Akbar, M Hasan, M Nazar, I Zulfahmi, E Miswar, M Iqhrammullah and Z Jalil. Fluorescent carbon quantum dots from Syzygium aromaticum as a selective sensor for Fe^{3+} and Cd^{2+} detection in

aqueous solution. *Case Studies in Chemical and Environmental Engineering* 2025; **11**, 101166.

[15] M Gao and Q Chang. Nonlinear absorption characteristics of carbon quantum dots. *Advances in Laser Technology and Applications* 2015; **9671**, 56-61.

[16] A Kolanowska, G Dzido, M Krzywiecki, MM Tomczyk, D Lukowiec, S Ruczka and S Boncel. Carbon quantum dots from amino acids revisited: Survey of renewable precursors toward high quantum-yield blue and green fluorescence. *ACS Omega* 2022; **7(45)**, 41165-41176.

[17] A Nair, JT Haponiuk, S Thomas and S Gopi. Natural carbon-based quantum dots and their applications in drug delivery: A review. *Biomedicine & Pharmacotherapy* 2020; **132**, 110834.

[18] P Namdari, B Negahdari and A Eatemadi. Synthesis, properties and biomedical applications of carbon-based quantum dots: An updated review. *Biomedicine & Pharmacotherapy* 2017; **87**, 209-222.

[19] F Limosani, EM Bauer, D Cecchetti, S Biagioni, V Orlando, R Pizzoferrato, P Prosposito and M Carbone. Top-down N-doped carbon quantum dots for multiple purposes: Heavy metal detection and intracellular fluorescence. *Nanomaterials* 2021; **11(9)**, 2249.

[20] KG Nguyen, IA Baragau, R Gromicova, A Nicolaev, SAJ Thomson, A Rennie, NP Power, MT Sajjad and S Kellici. Investigating the effect of N-doping on carbon quantum dots structure, optical properties and metal ion screening. *Scientific Reports* 2022; **12(1)**, 13806.

[21] J Dhariwal, GK Rao and D Vaya. Recent advancements towards the green synthesis of carbon quantum dots as an innovative and eco-friendly solution for metal ion sensing and monitoring. *RSC Sustainability* 2024; **2(1)**, 11-36.

[22] U Abd Rani, LY Ng, YS Ng, CY Ng, YH Ong and YP Lim. Photocatalytic degradation of methyl green dye by nitrogen-doped carbon quantum dots: Optimisation study by Taguchi approach. *Materials Science and Engineering: B* 2022; **283**, 115820.

[23] M Nazar, M Hasan, M Maghfira, S Mustiqillah, CE Nada, S Syahrial, K Puspita, R Rusman, NHH Abu Bakar and WS Althubaiti. Formulation of peel-off mask loaded with blue emissive carbon dots from *Hylocereus polyrhizus* peels as a UV-blocking active agent. *Results in Engineering* 2025; **27**, 105848.

[24] A Kaur, K Pandey, R Kaur, N Vashishat and M Kaur. Nanocomposites of carbon quantum dots and graphene quantum dots: Environmental applications as sensors. *Chemosensors* 2022; **10(9)**, 367.

[25] MJ Molaei. Principles, mechanisms, and application of carbon quantum dots in sensors: A review. *Analytical Methods* 2020; **12(10)**, 1266-1287.

[26] AJ Thibodeau, M Barret, F Mouchet, VX Nguyen and E Pinelli. The potential contribution of aquatic wildlife to antibiotic resistance dissemination in freshwater ecosystems: A review. *Environmental Pollution* 2024; **350**, 123894.

[27] MP Gomes. The convergence of antibiotic contamination, resistance, and climate dynamics in freshwater ecosystems. *Water* 2024; **16(18)**, 2606.

[28] C Manyi-Loh, S Mamphweli, E Meyer and A Okoh. Antibiotic use in agriculture and its consequential resistance in environmental sources: potential public health implications. *Molecules* 2018; **23(4)**, 795.

[29] MA Salam, MY Al-Amin, MT Salam, JS Pawar, N Akhter, AA Rabaan and MA Alqumber. Antimicrobial resistance: A growing serious threat for global public health. *Healthcare* 2023; **11(13)**, 1946.

[30] K Duan, G Pang, Y Duan, H Onyeaka and J Krebs. Current research development on food contaminants, future risks, regulatory regime and detection technologies: A systematic literature review. *Journal of Environmental Management* 2025; **381**, 125246.

[31] LTN Ngoc, JY Moon and YC Lee. Plant extract-derived carbon dots as cosmetic ingredients. *Nanomaterials* 2023; **13(19)**, 2654.

[32] MA Mousa, HH Abdelrahman, MA Fahmy, DG Ebrahim and AH Moustafa. Pure and doped carbon quantum dots as fluorescent probes for the detection of phenol compounds and antibiotics in aquariums. *Scientific Reports* 2023; **13(1)**, 12863.

[33] P Raji, AV Samrot, DB Rohan, MD Kumar, R Geetika, VK Sharma and D Keerthana. Extraction, characterization and *in vitro* bioactivity evaluation of alkaloids, flavonoids, saponins and tannins of cassia alata, *Thespesia populnea*, *Euphorbia hirta* and *Wrightia tinctoria*. *Rasayan Journal of Chemistry* 2019; **12(1)**, 123-137.

[34] M Usman and S Cheng. Recent trends and advancements in green synthesis of biomass-derived carbon dots. *Eng* 2024; **5(3)**, 2223-2263.

[35] N Javed and DM O'Carroll. Long-term effects of impurities on the particle size and optical emission of carbon dots. *Nanoscale Advances* 2021; **3(1)**, 182-189.

[36] Y Liu, CY Liu and ZY Zhang. Graphitized carbon dots emitting strong green photoluminescence. *Journal of Materials Chemistry C* 2013; **1(32)**, 4902-4907.

[37] S Chahal, JR Macairan, N Yousefi, N Tufenkji and R Naccache. Green synthesis of carbon dots and their applications. *RSC Advances* 2021; **11(41)**, 25354-25363.

[38] SS Makone and SN Niwadange. Green chemistry alternatives for sustainable development in organic synthesis. *International Advanced Research Journal in Science, Engineering and Technology* 2016; **3(6)**, 114-118.

[39] K Sato, R Katakami, Y Iso and T Isobe. Surface-modified carbon dots with improved photoluminescence quantum yield for color conversion in white-light-emitting diodes. *ACS Applied Nano Materials* 2022; **5(6)**, 7664-7669.

[40] M Nazar, CE Nada, S Syahrial, R Rusman, I Khaldun, M Hasan, B Wirjosentono and B Basri. Carbon quantum dots synthesis optimization using response surface methodology. *AIP Conference Proceedings* 2024; **3082(1)**, 040016.

[41] L Cao, X Wang, MJ Meziani, F Lu, H Wang, PG Luo, Y Lin, BA Harruff, LM Veca, D Murray, SY Xie and YP Sun. Carbon dots for multiphoton bioimaging. *Journal of the American Chemical Society* 2007; **129(37)**, 11318-11319.

[42] Z Peng, X Han, S Li, AO Al-Youbi, AS Bashammakh, MS El-Shahawi and RM Leblanc. Carbon dots: Biomacromolecule interaction, bioimaging and nanomedicine. *Coordination Chemistry Reviews* 2017; **343**, 256-277.

[43] A Hajji, PED Soto Rodriguez, A Souemti, L Wang, IR Martin and A Megriche. Optical ratiometric probes based on photoluminescent core-shell structured carbon dots@silica for temperature sensing. *Journal of the American Ceramic Society* 2026; **109(1)**, e70278.

[44] S Parveen, R Misra and SK Sahoo. *Nanoparticles: A boon to drug delivery, therapeutics, diagnostics and imaging. In*: L Balogh (Ed.). Nanomedicine in cancer. Jenny Stanford Publishing, New York, 2017, p. 47-98.

[45] P Chaudhary, A Verma, A Mishra, D Yadav, K Pal, BC Yadav, E Ranjith Kumar, KB Thapa, S Mishra and DK Dwivedi. Preparation of carbon quantum dots using bike pollutant soot: Evaluation of structural, optical and moisture sensing properties. *Physica E: Low-dimensional Systems and Nanostructures* 2022; **139**, 115174.

[46] BK John, AR Chacko, C Mohan and B Mathew. A review on carbon quantum dot based semiconductor photocatalysts for the abatement of refractory pollutants. *ChemPhysChem* 2022; **23(12)**, e202100873.

[47] YP Sun, B Zhou, Y Lin, W Wang, KAS Fernando, P Pathak, MJ Meziani, BA Harruff, X Wang, H Wang, PG Luo, H Yang, ME Kose, B Chen, LM Veca and SY Xie. Quantum-sized carbon dots for bright and colorful photoluminescence. *Journal of the American Chemical Society* 2006; **128(24)**, 7756-7757.

[48] A Kolanowska, G Dzido, M Krzywiecki, MM Tomczyk, D Lukowiec, S Ruczka and S Boncel. Carbon quantum dots from amino acids revisited: Survey of renewable precursors toward high quantum-yield blue and green fluorescence. *ACS Omega* 2022; **7(45)**, 41165-41176.

[49] A Nair, JT Haponiuk, S Thomas and S Gopi. Natural carbon-based quantum dots and their applications in drug delivery: A review. *Biomedicine & Pharmacotherapy* 2020; **132**, 110834.

[50] T Chatzimitakos and C Stalikas. *Antimicrobial properties of carbon quantum dots. In*: S Rajendran, A Mukherjee, TA Nguyen, C Godugu and RK Shukla (Eds.). Nanotoxicity. Elsevier, Amsterdam, Netherlands, 2020, p. 301-315.

[51] MS Zaini, LY Jian, JYC Liew and MA Kamarudin. Impact of carbon concentration on optical and zeta potential properties of carbon quantum dots. *Fullerenes, Nanotubes and Carbon Nanostructures* 2024; **32(11)**, 1039-1049.

[52] A Navidfar, MI Peker, E Budak, C Unlu and L Trabzon. Carbon quantum dots enhanced graphene/carbon nanotubes polyurethane hybrid nanocomposites. *Composites Part B: Engineering* 2022; **247**, 110310.

[53] NA Nazibudin, MF Zainuddin and CC Abdullah. Hydrothermal synthesis of carbon quantum dots: An updated review. *Journal of Advanced Research in Fluid Mechanics and Thermal Sciences* 2023; **101(1)**, 192-206.

[54] J Zheng, Y Xie, Y Wei, Y Yang, X Liu, Y Chen and B Xu. An efficient synthesis and photoelectric properties of green carbon quantum dots with high fluorescent quantum yield. *Nanomaterials* 2020; **10(1)**, 82.

[55] K Anpalagan, H Yin, I Cole, T Zhang and DT Lai. Quantum yield enhancement of carbon quantum dots using chemical-free precursors for sensing Cr (VI) ions. *Inorganics* 2024; **12(4)**, 96.

[56] D Kumar, K Singh, V Verma and HS Bhatti. Synthesis and characterization of carbon quantum dots from orange juice. *Journal of Bionanoscience* 2014; **8(4)**, 274-279.

[57] L Pan, S Sun, A Zhang, K Jiang, L Zhang, C Dong, Q Huang, A Wu and H Lin. Truly fluorescent excitation-dependent carbon dots and their applications in multicolor cellular imaging and multidimensional sensing. *Advanced Materials* 2015; **27(47)**, 7782-7787.

[58] MM Mata-Miranda, M Guerrero-Ruiz, JR Gonzalez-Fuentes, CM Hernandez-Toscano, JR Garcia-Andino, M Sanchez-Brito and GJ Vazquez-Zapien. Characterization of the biological fingerprint and identification of associated parameters in stress fractures by FTIR spectroscopy. *BioMed Research International* 2019; **2019(1)**, 1241452.

[59] A Debnath, MN Uddin, RA Jahan, AA Rana and MM Karim. Development of methods for quantification and classification of gelatin in capsule shell using chemometric analysis of FTIR spectroscopic data. *Bangladesh Journal of Scientific and Industrial Research* 2022; **57(2)**, 91-98.

[60] M Sudolska, M Dubecky, S Sarkar, CJ Reckmeier, R Zboril, AL Rogach and M Otyepka. Nature of absorption bands in oxygen-functionalized graphitic carbon dots. *The Journal of Physical Chemistry C* 2015; **119(23)**, 13369-13373.

[61] V Arul and MG Sethuraman. Hydrothermally green synthesized nitrogen-doped carbon dots from *Phyllanthus emblica* and their catalytic ability in the detoxification of textile effluents. *ACS Omega* 2019; **4(2)**, 3449-3457.

[62] E Dhandapani, N Duraisamy and P Periasamy. Highly green fluorescent carbon quantum dots synthesis via hydrothermal method from fish scale. *Materials Today: Proceedings* 2020; **26**, A1-A5.

[63] Y Xie, D Cheng, X Liu and A Han. Green hydrothermal synthesis of N-doped carbon dots from biomass highland barley for the detection of Hg^{2+}. *Sensors* 2019; **19(14)**, 3169.

[64] ZM Khan, RS Rahman, S Islam and M Zulfequar. Hydrothermal treatment of red lentils for the synthesis of fluorescent carbon quantum dots and its application for sensing Fe^{3+}. *Optical Materials* 2019; **91**, 386-395.

[65] S Elkun, M Ghali, T Sharshar and MM Mosaad. Green synthesis of fluorescent N-doped carbon quantum dots from castor seeds and their applications in cell imaging and pH sensing. *Scientific Reports* 2024; **14(1)**, 27927.

[66] Y Deng, M Chen, G Chen, W Zou, Y Zhao, H Zhang and Q Zhao. Visible-ultraviolet upconversion carbon quantum dots for enhancement of the photocatalytic activity of titanium dioxide. *ACS Omega* 2021; **6(6)**, 4247-4254.

[67] C Liu, F Zhang, J Hu, W Gao and M Zhang. A mini review on pH-sensitive photoluminescence in carbon nanodots. *Frontiers in Chemistry* 2021; **8**, 605028.

[68] RJ Murphy, D Pristinski, K Migler, JF Douglas and VM Prabhu. Dynamic light scattering investigations of nanoparticle aggregation following a light-induced pH jump. *The Journal of Chemical Physics* 2010; **132(19)**, 194903.

[69] J Li, W Wang, BL An, X Jia, YH Zhang, JR Li, YL Bai and JQ Xu. Luminescence color regulation of carbon quantum dots by surface modification. *Journal of Luminescence* 2022; **246**, 118811.

[70] H Shabbir, E Csapo and M Wojnicki. Carbon quantum dots: The role of surface functional groups and proposed mechanisms for metal ion sensing. *Inorganics* 2023; **11(6)**, 262.

[71] DA Hines and PV Kamat. Quantum dot surface chemistry: Ligand effects and electron transfer reactions. *The Journal of Physical Chemistry C* 2013; **117(27)**, 14418-14426.

[72] S Masha and O Samuel Oluwafemi. Cost-effective synthesis of red-emitting carbon-based quantum dots and its photothermal profiling. *Materials Letters* 2022; **325**, 132590.

[73] EO Chukwuocha, MC Onyeaju and TS Harry. Theoretical studies on the effect of confinement on quantum dots using the brus equation. *World Journal of Condensed Matter Physics* 2012; **2(2)**, 96-100.

[74] WH Melhuish. Quantum efficiencies of fluorescence of organic substances: Effect of solvent and concentration of the fluorescent solute. *The Journal of Physical Chemistry* 1961; **65(2)**, 229-235.

[75] D Ni, Q Shang, T Guo, X Wang, Y Wu, H Guan, D Wang and M Zhang. An effective strategy to improve dynamic and cyclic stability of HQC/TiO_2 photocatalyst by introducing carbon quantum dots or iron ion via metal-complex. *Applied Catalysis B: Environmental* 2017; **210**, 504-512.

[76] M Ghosh, L Madauss, M Schleberger, H Lebius, A Benyagoub, JA Wood and RG Lammertink. Understanding mono-and bivalent ion selectivities of nanoporous graphene using ionic and bi-ionic potentials. *Langmuir* 2020; **36(26)**, 7400-7407.

[77] C Bertei, E Bilotti and JE Gautrot. Anion-and Cation-Specific Response of the Aqueous Conformation of Strong and Weak Polyanionic Brushes. *Langmuir* 2025; **41(44)**, 29502-29515.

[78] M Dehghani, N Nasirizadeh and ME Yazdanshenas. Determination of cefixime using a novel electrochemical sensor produced with gold nanowires/graphene oxide/electropolymerized molecular imprinted polymer. *Materials Science and Engineering: C* 2019; **96**, 654-660.

[79] F Zu, F Yan, Z Bai, J Xu, Y Wang, Y Huang and X Zhou. The quenching of the fluorescence of carbon dots: A review on mechanisms and applications. *Microchimica Acta* 2017; **184(7)**, 1899-1914.

[80] H Qi, Z Zhai, X Dong and Z Zhang. Nitrogen doped carbon quantum dots (N-CQDs) with high luminescence for sensitive and selective detection of hypochlorite ions by fluorescence quenching. *Spectrochimica Acta Part A: Molecular and Biomolecular Spectroscopy* 2022; **279**, 121456.

[81] CE Enyoh, Q Wang, W Wang, M Suzuki, G Masuda, D Nakajima and S Lu. Green one-step synthesis and characterization of fluorescent carbon quantum dots from PET waste as a dual-mode sensing probe for Pd (II), ciprofloxacin, and fluoxetine via fluorescence quenching and enhancement mechanisms. *Surfaces* 2025; **8(2)**, 24.

[82] H Miao, Y Wang and X Yang. Carbon dots derived from tobacco for visually distinguishing and detecting three kinds of tetracyclines. *Nanoscale* 2018; **10(17)**, 8139-8145.

[83] RK Sajwan and PR Solanki. Gold@carbon quantum dots nanocomposites based 2-in-one sensor: A novel approach for sensitive detection of aminoglycosides antibiotics in food samples. *Food Chemistry* 2023; **415**, 135590.

[84] L Li, L Yang, D Lin, S Xu, M Mei, S Yu and C Jiang. Hydrogen-bond induced enhanced emission ratiometric fluorescent handy needle for visualization assay of amoxicillin by smartphone sensing platform. *Journal of Hazardous Materials* 2023; **444**, 130403.

[85] H Singh, S Singh, SK Bhardwaj, G Kaur, M Khatri, A Deep and N Bhardwaj. Development of carbon quantum dot-based lateral flow immunoassay for sensitive detection of aflatoxin M1 in milk. *Food Chemistry* 2022; **393**, 133374.

[86] X Lu, Q Gao, L Xu, Y Ren, F Tong, Y Wang, L Wang, N Ge and W Ge. Rapid determination of tetracycline utilizing a ratiometric fluorescence with Co-doped carbon quantum dots. *Journal of Food Composition and Analysis* 2025; **140**, 107252.

[87] L Ma, F Wang, Y Hua, Q Chen, M Zhang, Q Zhao, G Yang and Y Zhao. A ratiometric fluorescent nanoprobe for the specific and portable detection of tetracycline based on Eu/N, S-doped carbon dots. *Spectrochimica Acta Part A: Molecular and Biomolecular Spectroscopy* 2025; **336**, 127063.

[88] M Jie, A Zhu, J He, B Liu, X Yue, Z Xu and Y Bai. Smartphone-based fluorescence Eu/Ce-MOFs hydrogel sensor for sensitive and visual detection of tetracyclines with machine learning-assistance. *Food Chemistry* 2025; **493(1)**, 145721.

[89] S Asadi and N Ziraksaz. Dual mode fluorescence and spectrophotometric cefixime sensing using onion juice nitrogen doped carbon dots with smartphone and paper strip readouts. *Scientific Reports* 2025; **15**, 44626.

[90] ST Alsharif, AMBH Ali and MM El-Wekil. Colorimetric and fluorometric dual-mode sensing of cefadroxil based on peroxidase-like activity of iron and nitrogen co-doped carbon dots. *Spectrochimica Acta Part A: Molecular and Biomolecular Spectroscopy* 2025; **339**, 126313.

[91] R Pramudita, S Gea, A Daulay, M Harahap, YZ Tan, R Goei and AIY Tok. Synthesis of fluorescent citric acid carbon dots composites derived from empty fruit bunches of palm oil tree and its anti-bacterial property. *Case Studies in Chemical and Environmental Engineering* 2022; **6**, 100277.

[92] Q Zhang, Y Ao, J Liu, S Tang, F Tian, X Tian, X Luo and M Xie. Red-emissive carbon dot as fluorescent probe for the sensitive detection of sunset yellow in foodstuffs. *Food Chemistry* 2025; **463**, 141477.

[93] B Fu, Q Liu, M Liu, X Chen, H Lin, Z Zheng, J Zhu, C Dai, X Dong and DP Yang. Carbon dots enhanced gelatin/chitosan bio-nanocomposite packaging film for perishable foods. *Chinese Chemical Letters* 2022; **33(10)**, 4577-4582.

[94] G Ding, F Yan, S Yang and Y Fu. Recent advances in carbon quantum dots for antibiotics detection. *Reviews in Inorganic Chemistry* 2025; **45(1)**, 151-173.